Romanian Reports in Physics, Vol. 57, No. 4, P. 801–828, 2005

ATOMIC & MOLECULAR PHYSICS

QUANTUM INTERFERENCES OF SUPER-EXCITED STATES: APPLICATION TO ELECTRON-MOLECULAR CATION REACTIVE COLLISIONS

M. C. STROE[1,2], A. I. FLORESCU[3,4], M. FIFIRIG[1], F. O. WAFFEU TAMO[2,5], V. NGASSAM[5,6], O. MOTAPON[5], I. F. SCHNEIDER[2]

[1] *Department of Physics, Faculty of Chemistry, University of Bucharest, RO-70346, Bucharest, Romania*

[2] *Laboratoire de Mécanique, Physique et Géosciences, Université du Havre, F-76058, Le Havre, France*

[3] *Institute for Space Science, PO Box MG-36, RO-76900, Bucharest, Romania*

[4] *Laboratoire de Physique des Atomes, Lasers, Molécules et Surfaces (PALMS), Université de Rennes I, Campus de Beaulieu, F-35042, Rennes, France*

[5] *Center for Atomic, Molecular Physics and Quantum Optics, University of Douala, 00237, Douala, Cameroon*

[6]*Department of Applied Sciences, University of California, Davis, CA, USA*

(Received June 15, 2005)

Abstract. The theoretical description of different reactive collisions – dissociative recombination, dissociative excitation, elastic, inelastic and super-elastic collisions – of electrons with molecular cations is illustrated in terms of a method [1] based on the Multichannel Quantum Defect Theory [2–4]. We outline the various aspects of this approach – representations of molecular states (many of them, electronically or ro-vibrationally super-excited), channel interactions, mechanisms and competitive processes. The multi-channel character of the collisions, implying quantum interferences between zero-order states of the molecular system, is emphasized. We support these aspects with examples and applications on various diatomic molecular cations – H_2^+, HD^+, DT^+, HeH^+, and NO^+ – with electrons of energy between 0.01 meV and 13 eV. The computed cross sections and rate coefficients aim at providing input data for the kinetic modelling of ionized media of astrophysical, planetary, environmental and energetic interest.

Key words: quantum interferences, superexcited states, electrons, molecular cations, collisions.

1. INTRODUCTION

The modelling of various media of fundamental or technological interest – interstellar molecular clouds, supernovae, planetary atmospheres, plasma-assisted combustion and de-pollution, atmospheric re-entry of hypersonic spacecrafts, edge fusion plasma and plasma processing [5–15] is strongly based on the knowledge of

cross sections and rate coefficients of the elementary radiative and collisional processes.

One of the elementary processes which plays a decisive role in the ionization degree and in the energetics of plasmas containing *AB* molecules is the **dissociative recombination** (DR) of the molecular cations AB^+ with electrons:

$$AB^+\left(N_i^+, v_i^+\right) + e^-(\varepsilon) \rightarrow A + B\left(E\right) \tag{1}$$

Here N_i^+ and v_i^+ are the initial rotational and vibrational quantum numbers of the target molecular ion, ε is the energy of the incident electron and E is the inter-atomic kinetic energy release following the dissociation.

Actually, the DR process is just one of the possible ways out of the electron-cation collisions. Indeed, autoionization is always a competitive process with respect to the capture, resulting in **elastic** ($\varepsilon' = \varepsilon$, EC), **inelastic** ($\varepsilon' < \varepsilon$, IC) or **super-elastic** ($\varepsilon' > \varepsilon$, SEC) **collisions**:

$$AB^+\left(N_i^+, v_i^+\right) + e^-(\varepsilon) \rightarrow AB^+\left(N_f^+, v_f^+\right) + e^-(\varepsilon') \tag{2}$$

or, *above* the dissociation threshold of the cation, in **dissociative excitation** (DE):

$$AB^+\left(N_i^+, v_i^+\right) + e^-(\varepsilon) \rightarrow A + B^+\left(E\right) + e^-(\varepsilon') \tag{3}$$

In the last two decades, these reactive collisions, involving H_2^+ ($A = H$, $B = H$) HeH^+ ($A = He$, $B = H$), NO^+, H_3^+ ($A = H$, $B = H_2$), including some of their isotopomers, and many other diatomic or poly-atomic molecular ions have been actively studied, both experimentally and theoretically.

The most complete experiments on these ions in the last decade have been performed in ion storage rings [16–29] where molecular ions can be stored for several seconds and cooled by electronic collisions, thus allowing high resolution measurements of cross sections and branching ratios. With some notable exceptions [25–26], these experiments deal with fully vibrationally relaxed ions, since resolving the vibrational distribution in an ionic beam remains a difficult task. The rotational distribution is still a more complex subject and, in most cases, Boltzmann distribution is assumed, corresponding to some hundreds of Kelvin [20–21].

This article is an overview of the main theoretical concepts and methods used in the time-independent approach of the above-mentioned electron-cation collisions, with application to diatomic systems. We discuss in detail the key aspects of the modelling: Section 2 is devoted to the nature of the zero-order *states*, to their appropriate representations – quasi-diabatic or adiabatic – and to their corresponding mutual interactions – electronic or non-adiabatic respectively. Section 3 illustrates the main steps in the description of the reaction *dynamics* within the method of the Multi-channel Quantum Defect Theory (MQDT): the

identification of the reaction channels, the building of the interaction, reaction and scattering matrices. The quantum interferences of states – organized in ionization and dissociation channels, open or closed – are shown to explain the formation of temporary compound neutral states and, eventually, of the final neutral or charged products, with a cross section often dominated by Fano-type resonances. These ideas are applied to some diatomic systems – H_2, *HD*, *DT*, *HeH,* and *NO* – in Section 4. And finally, in Section 5, the conclusions and the perspectives of our work are presented.

2. THE MOLECULAR STATES AND THEIR MUTUAL INTERACTIONS

2.A. WHAT ARE THE STATES WE NEED?

DR is one of the simplest *reactive* collisions, and one of the most convincing examples of breakdown of the Born-Oppenheimer approximation [30, 31]: the dissociative capture is possible due to the existence of *interactions* between the dissociation and the ionization continua of molecular states. Actually, the latter type of continuum is completed by its extrapolation below threshold with the Rydberg bound states. Therefore, a more detailed description of reaction (1) reads:

$$AB^+\left(N_i^+,\ v_i^+\right) + e^-(\varepsilon) \rightarrow AB^{**}, \quad AB^* \rightarrow A + B(E) \tag{4}$$

where "**" stands for a dissociative electronic state, *i.e.*, a state whose separated-atom energy limit is situated *below* the initial ro-vibrational level of the target ion, and "*" for a bound Rydberg state. These two types of states of the neutral system are related to two mechanisms: the capture into an AB^{**} state is called *direct* DR, whereas the temporary capture into an AB^* state, followed by its quick predissociation by AB^{**}, is the *indirect* DR. These two mechanisms **quantally interfere** within the so-called *total* process, resulting in many series of Fano-type – or more complicated – resonances in the shape of the cross section [32, 1]. Notice that the electronic part of the AB^* and AB^{**} states are built either on ground, or on excited electronic state of the AB^+ ion.

Actually, more terms contribute to this kind of interference. The $(AB^+ + e^-)$ state in the left-hand side of the reactions (1–4), corresponding to their entrance channel, can be regarded as an extrapolation, beyond the ionization threshold, of the series of AB^* states. So do the $(AB^+ + e^-)$ states appearing in the right-hand side of the reactions (2), which describe one type of autoionization, namely that with respect to the *bound* ro-vibrational states of the ion. As for the reaction (3), it can be regarded as a second type of autoionization, occurring with respect to levels from the *continuum* part of the ro-vibrational spectrum, which one can call

dissociative autoionization [19, 33]. Meanwhile, (2) and (3) involve also *electronically* bound states of type AB^{**} and AB^{*}, which correspond to captures of the electron, competing electronic scattering and dissociative excitation.

As a matter of fact, *all* of these states have to be *simultaneously* included in every calculation, and it is their interference which will result in the various exit channels, corresponding to the different processes – DR, EC, IC, SEC and DE. But how can these states be built?

2.B. THE QUASI-DIABATIC REPRESENTATIONS AND THE ELECTRONIC INTERACTIONS

The most natural option would be to use electronic states belonging to the adiabatic representation. Within this choice, the states described above diagonalize

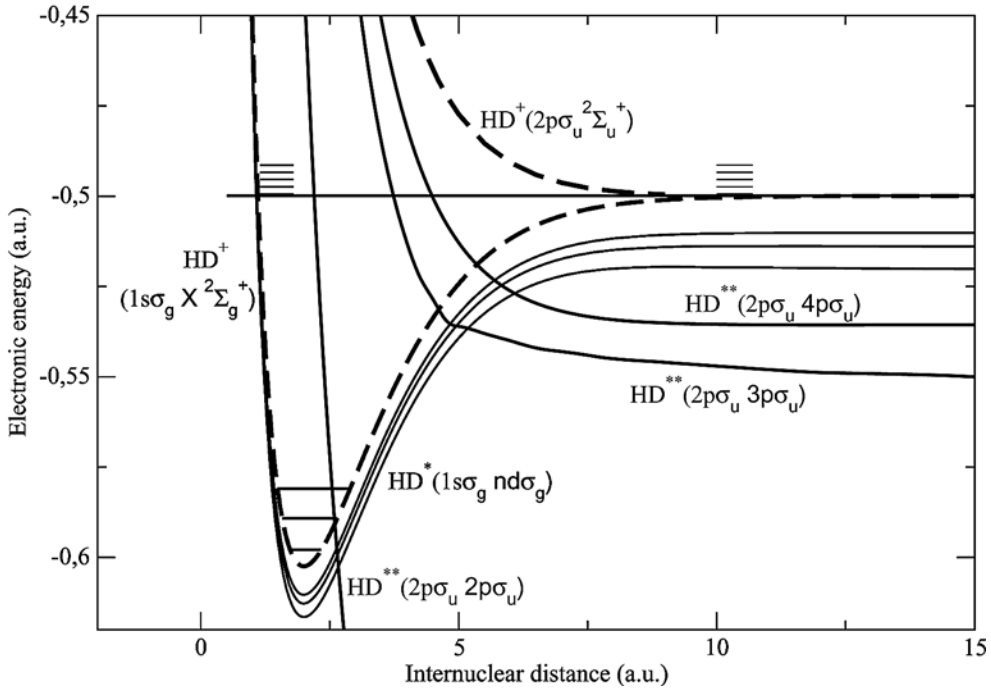

Fig. 1 – Quasi-diabatic representation of the *HD* super-excited states of $^1\Sigma_g^+$ symmetry. Some vibrational states of the HD^+ ground electronic state (black dashed curve) as well as some vibrational levels from the continuum part of its vibrational spectrum are represented as black horizontal lines. Some continuum-type vibrational levels of the HD^+ first electronically excited state (grey dashed curve) are represented as grey horizontal lines (no discrete part of the vibrational spectrum is available in this case). Some states belonging to a Rydberg series converging to the HD^+ ground state (black continuum curves) and, respectively, to the HD^+ first excited state (grey continuum curves) are represented (the molecular data are those used in [34]).

the electronic Hamiltonian, and can be coupled through the kinetic energy operator (non-adiabatic couplings). As it will be shown later, this could be indeed the right choice for some systems.

However, historically, for many years, describing DR within this "traditional" representation faced a severe obstacle for the case of NO^+ [30, 31] and other numerous diatomic or poly-atomic cations which strongly recombine. The reason for this was the fact that the relevant adiabatic states display, within a given symmetry and for some inter-nuclear distances, avoided crossings, and that the non-adiabatic interactions are so large around these regions that they prevent a perturbative solution of the coupled equation system resulting from the Schrödinger equation. Moreover, these non-adiabatic couplings – matrix elements of the kinetic energy operator involving electronic states – were, and are still, difficult to compute.

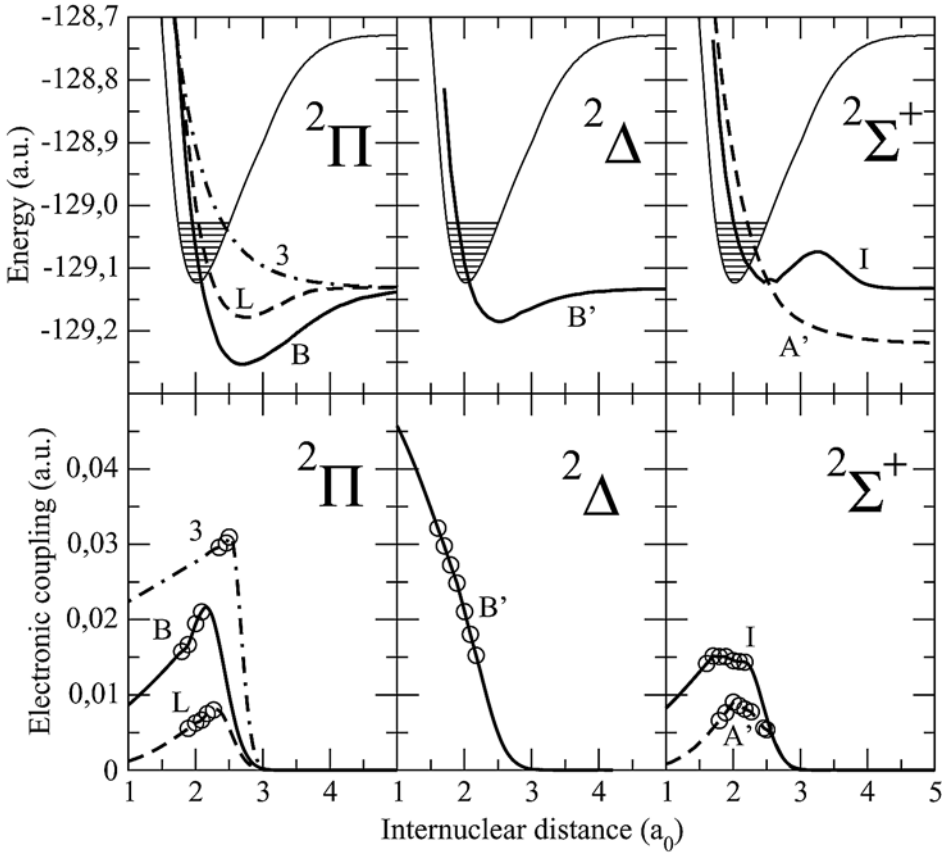

Fig. 2 – Quasi-diabatic representation of *NO* super-excited states of all the relevant symmetries. Some vibrational states of the NO^+ ground electronic state (fine continuous curve) are represented as black horizontal lines. The circles label values of the scaled electronic couplings computed by the *R*-matrix method [36, 37].

Instead, quasi-diabatic representations [35] have been successfully employed. Within these representations, in which the curves of the same symmetry are allowed to cross, it is the kinetic energy operator which is diagonalized, whereas the electronic part of the molecular Hamiltonian is only *partially* diagonalized, within subspaces of states associated to the same ionic electronic core. Consequently, the matrix elements of this Hamiltonian, coupling electronic states built on different ionic electronic cores, do not vanish, providing what is currently called *electronic* interactions.

Fig. 1 illustrates some of these states for the most simple system, HD^+/HD, whereas Fig. 2, corresponding to NO^+/NO system, provides also the electronic couplings between each dissociative state and the ionisation continuum. Notice that the crossings between the ion potential curve and the dissociative states – occurring in these figures – grant a good overlap between the inter-nuclear wave-functions of the vibrational states whose energy levels are close to the crossings, and the dissociative states and, consequently, a high recombination rate for the ions on these levels. This crossings have their origin in the quasi-diabatic nature of the states, namely on the allowed crossings between highly-excited Rydberg states and the dissociative ones.

2.C. THE ADIABATIC REPRESENTATION AND THE NON-ADIABATIC INTERACTIONS

Many molecules do not display avoided crossings between the Born-Oppenheimer states and therefore, they can be studied within the adiabatic representation. At the beginning of the nineties, one of the most challenging aspects of the DR was the study of systems *without* a curve crossing between the ion electronic ground state and a dissociative electronic state of the neutral molecule. Among these systems, HeH^+ is the simplest heterogeneous molecular ion and was probably the first molecular species to be produced in the early universe [38]. *A priori*, the DR cross section is expected to be small [39, 40] due to the lack of a curve crossing in the vicinity of the ion ground state minimum. But in the first experimental study of the DR of $^4HeH^+$ [42] the cross section was found *not* to be small, having a value of 3×10^{-15} *cm*^{2} at *0.01 eV* and falling off to near zero above *0.1 eV*. A striking feature of these measurements was what appeared to be a deep window resonance observed at *0.03 eV*. Later measurements by various groups [43] confirmed the unexpectedly high DR cross sections at low energy, and prompted a number of theoretical studies [44–47].

It was proposed that the large cross section values could be explained by *radial* , *i.e. non-adiabatic* coupling of the initial (ion + electron) state to underlying Rydberg states that could undergo dissociation and thus stabilize the collision. Early MQDT calculations [44] involved the coupling of the ionisation continuum to the *C* and *D* states of neutral *HeH* (Fig. 3) and predicted that the final state products

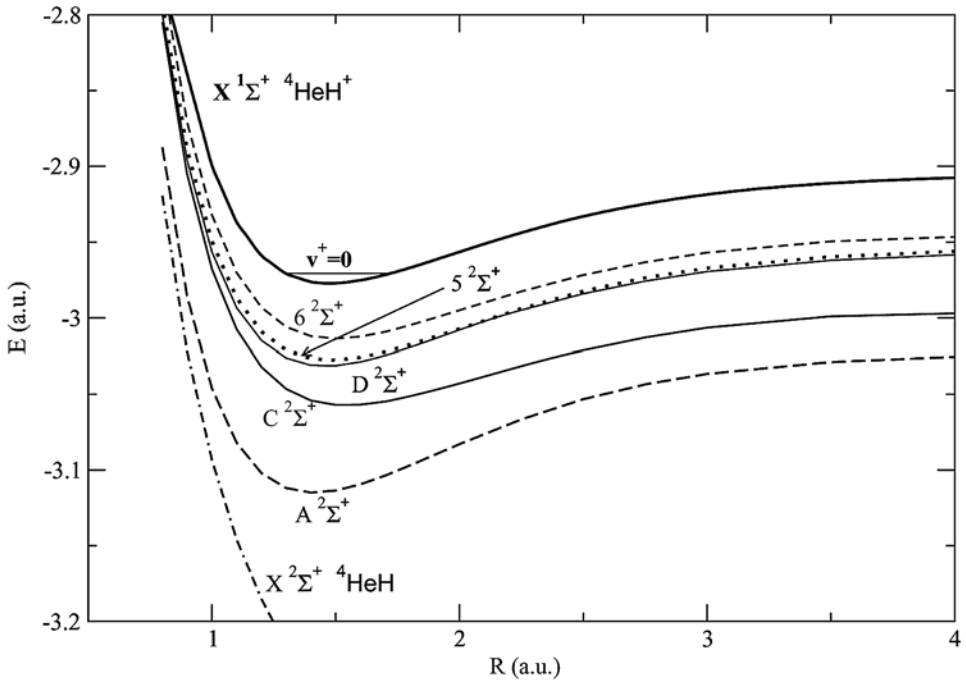

Fig. 3 – Selected electronic potential energy curves for *HeH* and HeH^+ correlating at large *R* with *H*, *n* = 1, 2 and 3 [41].

would be *He* + *H* (*n* = 2). An almost simultaneous R-matrix approach [46] considered coupling to the *A* and *X* states, that would yield *He* + *H* (*n* = 1) products. Experimental measurements [48] settled this question by observing that at low energy all the products were formed in the *He* + *H* (*n* = 2) channel. Still, the theoretical results were not giving a clear answer about the mechanism of the DR driven by non-adiabatic couplings. This lack of transparency owes to the details of the MQDT methods used. Explicit radial couplings between bound-bound states of the neutral molecule extrapolated to the bound-continuum were employed [44, 45], while only adiabatic quantum defects of the dissociative states are needed in more recent MQDT studies [47, 49] which, moreover, include rotation (see Section 4).

Motivated by these questions, we decided to perform an MQDT calculation without rotation [50], as performed in [44, 45] but with different radial couplings: based on a recently derived [51] generalized Hellman-Feynman theorem, regular radial coupling effects can be treated explicitly. Within the framework of the MQDT, the bound-bound formula [51] for the radial coupling, in the simple case of two *ab initio* Born-Oppenheimer states, members of the same Rydberg series, can be analytically extrapolated [52] to the bound-continuum coupling between an $nl\Lambda$ electronic bound state and the ε electronic continuum, Λ being the projection of the total angular momentum on the inter-nuclear axis. We have already used this

method [41] (to be referred to as paper I) to evaluate the radial couplings of some Rydberg $^3\Sigma$ and $^3\Pi$ states of H_2. In that case, we have predicted measurable cross sections, but smaller by at least one order of magnitude than the typical DR cross section corresponding to capture into a doubly excited state which do cross the ion ground state.

Thus, we found it worthwhile to re-examine the molecular potentials and the radial couplings involved in the HeH^+ DR. The HeH^+-electron system is similar to that treated in paper I. Breakdown of the Born-Oppenheimer approximation occurs for the C state which is a 3*s* Rydberg at short distance and achieves a 2*p* character while evolving toward the asymptotic *He* ($1s^2$) + *H* (2*p*) limit, as it does for the *h* $^3\Sigma_g^+$ H_2 which evolves from 3*s* to 2*p*.

Fig. 3 shows the lowest $^2\Sigma^+$ states dissociating to the *He* ($1s^2$) + *H* (n = 1, 2, 3) asymptotic limit. They are the result of a multi-reference configuration interaction calculation [44]. The possible dissociative routes at low electron-energy are the *X, A* and *C* states converging to the *H* (n = 1, 2) asymptotic limit. All the other states converging to the *H* (n = 3) asymptotic limit are closed for DR at low electron energy.

Our calculations [50] confirmed that the *C* $^2\Sigma^+$ state is the dominant dissociative route, as was found previously [44, 45]. However, as we will show in Section 4, our cross section is about two orders of magnitude smaller than the one calculated in [44, 45]. On the other hand, the most recent MQDT approach [47] demonstrates the contribution of the rotation to the DR cross section and confirms that the result we obtained is correct, as a model calculation neglecting rotation. In order to support these result, we shall give here some details about the way in which we construct the radial non-adiabatic coupling [51].

We have built up radial couplings between the *C* dissociative state and the electronic continuum assuming that the *C* state is a 3*s* Rydberg at short internuclear distance. The next member of this *s* $^2\Sigma^+$ series is the n = 4 state (6 $^2\Sigma^+$ in Fig. 3). We neglect the *l*-mixing with the *p* $^2\Sigma^+$ series, assuming the one-channel model [1, 54] to be valid. Thus, the Rydberg formula [55]:

$$U_{nl\Lambda}^{neutral}(R) = U_{gs}^{ion}(R) - \frac{1}{2[n - \mu_l^{\Lambda}(R)]^2} \tag{5}$$

(in a.u.) allows us to extract the quantum defect of the 6 $^2\Sigma^+$ state which we will consider as the *s* series (practically) constant quantum defect, $\mu_l^{\Lambda}(R)$, characterizing the super-excited Rydberg states. In Fig. 4 we show the quantum defects for the *A, C, D, 5* and 6 $^2\Sigma^+$ *HeH* states. Indeed, we see that the *C* and *6* state's quantum defects have the same *R*-dependence, but, being the lowest members of the *s* series, they still carry some energy dependence.

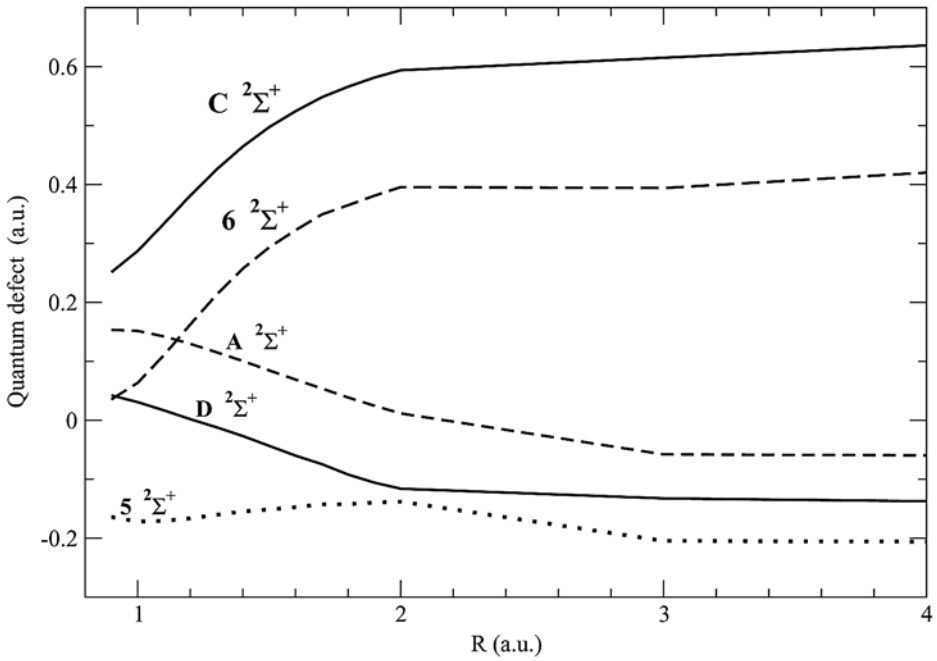

Fig. 4 – Quantum defects corresponding to the $^2\Sigma^+$ potential curves presented in Fig. 3.

We then calculate the radial coupling (in a.u.) between the *C* state ($n = 3$) and the continuum εs ($l = 0$):

$$B^{\Lambda}_{n\varepsilon l}(R) = \frac{2\dfrac{\partial \mu^{\Lambda}_l(R)}{\partial R}\nu_n^{\frac{1}{2}}}{(1+C_n)^{\frac{1}{2}}(1+2\varepsilon\nu_n^2)} \tag{6}$$

where $\nu_n = n - \mu^{\Lambda}_l$ is the effective quantum number of the n^{th} member of the fixed l series, and μ^{Λ}_l the corresponding quantum defect; $C_n = \dfrac{2}{\nu_n^2}\dfrac{\partial \mu^{\Lambda}_l}{\partial \varepsilon_n}$ is a small correction which cancel out in the $\nu_n \to \infty$ limit.

As can be seen in Fig. 5, the differences between the radial matrix element calculated using the C state quantum defect and that calculated using the 6 state quantum defect in equation (6) are minor. They have the same order of magnitude and a maximum located at about the same distance, as expected from the similar shapes of the corresponding quantum defects (see Fig. 4).

We have also considered the *A* state coupling to the continuum. The *A* state has a *2p* character at short distance, and the next member of the series is the *D* state, of character *3p* at short distance. Equation (6) gives a very small radial coupling, three times smaller than the *C* state coupling. Combined with the fact that

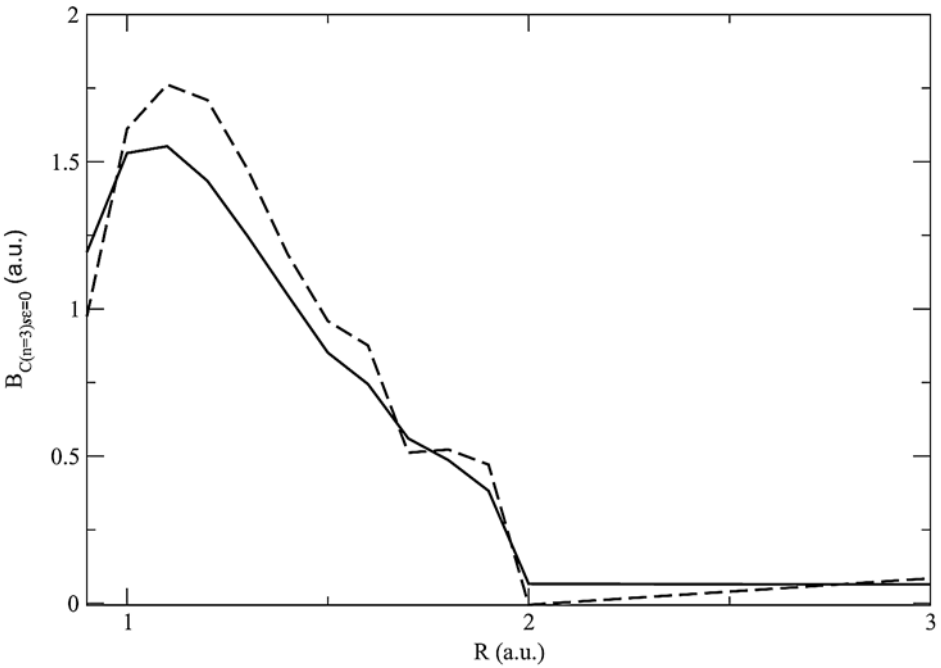

Fig. 5 – Radial matrix elements between the C dissociative state and the ionisation continuum using the C state quantum defect (full line) and the 6 state quantum defect (dashed line) at zero electron energy.

the *A* state nuclear wave function has a smaller overlap with the ion ground state nuclear wave function than the *C* state one, it is clear that the DR cross section is negligible for the *A* state (see Sections 3 and 4).

3. THE MOLECULAR DYNAMICS, DESCRIBED WITHIN THE MQDT FORMALISM

On the theoretical side, many of the studies of the DR and related electron/molecular cation collisions are based on the method of Annick SUZOR-WEINER [1, 54, 56] emerging from the MQDT [2, 3, 57–59]. Many of the authors of the present article [33, 34, 41, 50, 60–70] worked in – or collaborated with – SUZOR-WEINER's group in Orsay and, on the other hand, many other MQDT developments and calculations started from her pioneer studies [44, 45, 71].

One should also mention the time-dependent (wave packet) approach, a very powerful method, which still does not handle entirely all the resonant aspects of the collisions [65, 73–77]. The R-matrix approach was much less used in the study of these reactive processes [46], being rather complementary to the MQDT and

providing to this latter the input ingredients necessary for the description of the dynamics of the relevant super-excited states [78].

The main steps of the MQDT treatment of the electron – molecular cation collisions are briefly summarized here, following more detailed previous descriptions [71, 78, 33, 66]. Since all the reactive processes of interest are treated simultaneously within the same calculation, we shall restrict ourselves to a brief description of the obtention of the DR cross section.

Dissociative recombination is a multi-channel reactive collision involving two types of ***channels***: *ionization* channels (electron-molecular ion scattering, among which is the entrance channel) and *dissociation* ones (atom-atom scattering).

In the outer region of the reaction zone (region A [79]), the Born-Oppenheimer picture is appropriate for a zero-order representation of the neutral (electron + ion) system. The *ionization* channels – each of them spanning a Rydberg series of monoexcited states – are labeled by:

N, M, Λ – quantum numbers associated to the total orbital angular momentum and its projections on the z-axis of the laboratory-fixed and of the molecule-fixed frame respectively;

ℓ – orbital quantum number of the excited electron;

v – vibrational quantum number of the bound nuclear motion for this channel.

The *dissociation* channels consist of well determined dissociative states characterized by similar N, M, Λ quantum numbers and by a collective index d_j ($j = 1,\ N_{d\Lambda}$) which describes the relevant electronic configuration. For both types of channels corresponding to the same pair (N, Λ), the centrifugal term, proportional to $\left[N(N+1)-\Lambda^2\right]/R^2$ (where R is the internuclear distance) must be added to the electronic potential for the calculation of the radial nuclear wave functions, bound and dissociative.

The *electronic* coupling between the two types of channels is determined by the interaction matrix $\mathbf{V}$, **diagonal** in N, M and Λ. The 'on the energy-shell' elements of $\mathbf{V}$, corresponding to the *total* energy E, can be expressed as:

$$\mathbf{V}^{NM\Lambda}_{d_j,\ell v}(E,E) = V^{NM\Lambda}_{d_j,\ell v}(E) = \left\langle \chi^{\Lambda}_{d_j} \left| V^{(e)}_{d_j,\ell\Lambda} \right| \chi^{\Lambda}_{Nv} \right\rangle \tag{7}$$

The above bracket is an integral over the internuclear distance. χ^{Λ}_{Nv} and $\chi^{\Lambda}_{d_j}$ are nuclear radial wave-functions corresponding to a bound and to a dissociative state, respectively. The matrix elements $V^{(e)}_{d_j,\ell\Lambda}(R)$ express the strength of the configuration interaction between the dissociative state $d_j\Lambda$ and *each* member of the $\ell\Lambda$ – Rydberg series of monoexcited neutral states, and are computed by

numerical integration on the electronic coordinates of the specific interaction operators – local in the case of the quasi-diabatic representation (Fig. 1) and non-local in the case of the adiabatic representation (eq. (6) and Fig. 5) – described in Section 2.

In fact, the total angular momentum and its projection on the *z*-axis of the laboratory-fixed frame are constants of motion, and therefore, we shall restrict our discussion to a single pair *N*, *M*. In contrast, we have to include simultaneously the contributions of all the possible values of Λ, the projection of the total angular momentum on the z-axis of the molecular frame.

Starting from $\mathbf{V}$ one can build the reaction matrix $\mathcal{K}$:

$$\mathcal{K} = \mathcal{V} + \mathcal{V}\boldsymbol{G_0}\mathcal{K} \tag{8}$$

whose energy diagonal part:

$$\mathcal{K}(E, E) = \boldsymbol{K}(E) \tag{9}$$

leads to the construction of a configuration-interaction type basis set:

$$\psi^{(A)} = \left(\mathbf{1} + \boldsymbol{G_0}\boldsymbol{K}\right)\varphi^{(A)} \tag{10}$$

In the above equations, $\boldsymbol{G_0}$ is the non-local Green operator associated with the zero order Hamiltonian [54], namely $\frac{\boldsymbol{P}}{E - \mathbf{H_0}}$, where $\boldsymbol{P}$ denotes the principal value operator, and $\varphi^{(A)}$ and $\psi^{(A)}$ are basis-set wave-functions corresponding to the zero-order and actual Hamiltonian, respectively. The evaluation of the reaction matrix $\mathcal{K}$, *i.e.* the numerical solution of the Lippman-Schwinger equation (8) is described in detail in a recent article [69].

In order to express the result of the short-range interaction in terms of phase-shifts, a further change of basis set is performed:

$$\tilde{\psi}^{(A)} = \cos(\eta)\boldsymbol{U}^{\mathbf{T}}\psi^{(A)} \tag{11}$$

where the unitary matrix $\boldsymbol{U}$ and the diagonal matrix of phase-shifts $\boldsymbol{\eta}$ are the solution of the eigenvalue problem associated with the reaction matrix:

$$\pi\boldsymbol{K}\boldsymbol{U} = -\tan(\eta)\boldsymbol{U} \tag{12}$$

The block-diagonal structure of the interaction matrix with respect to Λ is transmitted to the reaction matrix. Consequently, the preceding equations (7–12) apply *independently* in *each* Λ-*subspace*. The Λ-mixing occurs only in the external zone, where Λ ceases to be a good quantum number (transition from Hund's case (b) to case (d) [58]). The other parameters (ℓ, v, d_j) take in these equations all the possible values according to angular momentum algebra and conservation of

energy, compatible with the given values of N, M and E. These latter quantities will not be displayed, unless necessary, in the forthcoming equations.

In the external zone (region B [79]), for larger electron-core distances, the Born-Oppenheimer picture is no more valid for the ionization channels because the external electron becomes weakly coupled to the core electrons. A close-coupling representation of the type "molecular ion + electron in Coulomb field" becomes appropriate, and these channels will be labelled by:

N, M – constants of motion, with the same meaning as in the A region;
ℓ – orbital quantum number of the electron in the Coulomb field;
N^+, M^+, Λ^+ – quantum numbers associated with the total orbital angular momentum of the molecular ion and its projections on the z-axis of the laboratory-fixed and of the molecule-fixed frame, respectively;
v^+ – vibrational quantum number of the molecular ion.

The dissociative channels are the same as in region A, which is distinct from the B region only for the Rydberg configurations with an external electron coupled to (region A) or uncoupled from (region B) the core electronic cloud.

Although the critical zone for the recombination process is the internal region A, the actual eigenfunction also has to be expressed in the close-coupling representation used in the external region (B), where the collision channels may be defined. The corresponding projection coefficients are:

$$C_{\ell N^+ v^+,\Lambda\alpha} = \left(\frac{2N^+ + 1}{2N+1}\right)^{1/2} \left\langle l(\Lambda - \Lambda^+) N^+ \Lambda^+ \middle| l N^+ N \Lambda \right\rangle \cdot$$
$$\cdot \frac{1 + \tau^+ \cdot \tau (-1)^{N-\ell-N^+}}{\left[2(2-\delta_{\Lambda^+,0})(1+\delta_{\Lambda^+,0}\delta_{\Lambda,0})\right]^{1/2}} \cdot \sum_v U^{\Lambda}_{\ell v,\alpha} \left\langle \chi_{N^+,v^+} \middle| \cos\left\{\pi\mu_{\ell\Lambda}(R) + \eta^{\Lambda}_{\alpha}\right\} \middle| \chi^{\Lambda}_{N,v} \right\rangle \tag{13}$$

$$C_{d,\Lambda\alpha} = U^{\Lambda}_{d,\alpha} \cos\eta^{\Lambda}_{\alpha} \tag{14}$$

as well as $S_{N^+\ell v^+,\Lambda\alpha}$ and $S_{d,\Lambda\alpha}$, obtained from equations (13) et (14) by replacing "cos" by "sin". The $\chi_{N^+v^+}$ and χ^{Λ}_{Nv} are the vibrational wave functions of the ground state molecular ion in the (N^+, v^+) ro-vibrational level and of a Rydberg monoexcited state in the (N, v) ro-vibrational level respectively, and $\mu_{\ell\Lambda}(R)$ is the electronic quantum defect characterizing these $l\Lambda$ – Rydberg series. For a given Λ, the index α denotes the eigenchannels defined through the diagonalization of the electronic reaction sub-matrix K^{Λ}, with eigenvalues $-\frac{1}{\pi}\tan(\eta^{\Lambda}_{\alpha})$ and eigenvectors ($U^{\Lambda}_{lv,\alpha}$, $U^{\Lambda}_{d,\alpha}$). Each block K^{Λ} of the reaction matrix is evaluated from the electronic coupling functions $V^{\Lambda}(R)$ between singly and doubly excited configurations with Λ symmetry [33, 34, 67]. The quantities τ^+ and τ (with values ± 1) are related to the

reflection symmetry of the ion and neutral wave function respectively, and take the values +1 for symmetric states and –1 for anti-symmetric ones [68]. The ratio in front of the sum in the right hand side of equation (13) contains the selection rules for the rotational quantum numbers.

These projection coefficients express the two types of couplings which control the process: the coupling between the dissociation and ionisation channels (electronic or non-adiabatic, see Section 2), expressed by the elements of the matrices $\boldsymbol{U}$ and η, and the **rovibronic** coupling between ionisation channels, through the R-dependence of the quantum defect $\mu_{\ell\Lambda}(R)$ and the angular mixing coefficients.

The matrices $\mathcal{C}$ and $\mathcal{S}$, whose elements are given by equations (13) and (14), are the basic blocks for the construction of the generalized scattering matrix **X** [2]:

$$\mathbf{X} = \frac{\mathcal{C} + i\mathcal{S}}{\mathcal{C} - i\mathcal{S}} \tag{15}$$

The **S** scattering matrix restricted to the *open* channels (not to be confounded with the frame-transformation $\mathcal{S}$ matrix appearing eq. 15) is [2]:

$$\mathbf{S} = \mathbf{X_{oo}} - \mathbf{X_{oc}} \left(\mathbf{X_{cc}} - e^{-2i\pi\nu} \right)^{-1} \mathbf{X_{co}} \tag{16}$$

It is obtained from sub-matrices of **X** involving rows and columns associated with open (o) or closed (c) channels, and a diagonal matrix formed with the effective quantum numbers $\nu_{N^+v^+} = 1/\sqrt{2 \cdot (E_{N^+v^+} - E)}$ (in a.u.) associated with each rovibrational ion threshold $E_{N^+v^+}$ located *above* the current energy E.

The scattering matrix elements enter directly into the expression of the partial cross section associated with a dissociative state d_{0j} with quantum parameters [*sym*, N, Λ_0] where « sym » summarizes all the additional symmetry characters (*e.g.*, spin multiplicity, parity (±) and, in the case of homonuclear molecules, g/u symmetry). For a molecular ion in the initial level $N_i^+ v_i^+$ recombining with an electron of energy ε, this partial cross section is given (in atomic units) by:

$$\sigma^{N,sym}_{\Lambda_0 d_{0j} \leftarrow N_i^+ v_i^+} = \frac{\pi}{4\varepsilon} \rho^{\Lambda_0, d_{0j}, sym} \frac{2N+1}{2N_i^+ + 1} \sum_{\ell} \left| S^{N,sym}_{\Lambda_0 d_{0j} \leftarrow \ell N_i^+ v_i^+} \right|^2 \tag{17}$$

where $\rho^{\Lambda_0, d_{0j}, sym}$ is the ratio between the multiplicities of the neutral and the ionic electronic states.

Finally, we have to make the summation over all the [*sym*, N, Λ_0, j] parameters:

$$\sigma_{diss \leftarrow N_i^+ v_i^+} = \sum_{sym} \sum_{N} \sum_{\Lambda_0} \sum_{j} \sigma^{N,sym}_{\Lambda_0 d_{0j} \leftarrow N_i^+ v_i^+} \tag{18}$$

in order to obtain the total DR cross section for a given ro-vibrational initial state of the molecular ion.

At high energy, the effect of the continuum part of the vibrational spectrum of the molecular ion – which formally is present in the preceding formulas if we extrapolate the v^+ *bound* vibrational states to states from the vibrational *continuum* – plays a very important role.

The most striking effect is the occurence – at the dissociation threshold of the ion – of the dissociative excitation – eq. (3) – which is the extension into the vibrational continuum of the vibrational excitation. Whereas in the past, a first order approach was used to estimate the magnitude of this process, as well as its influence on the DR [19, 33, 83], a more rigorous method allows us today to consider it via the "quasi-discretization" of the continuum, using the procedure introduced by Takagi [84]:

$$\chi_{E_i}(R) = \frac{1}{\sqrt{\Delta}} \int_{E_i-\Delta/2}^{E_i+\Delta/2} \chi_E(R)\,\mathrm{d}E, \qquad \Delta = E_{i+1} - E_i \tag{19}$$

where the vibrational continuum labelled by the energy E is divided in a number of bands of width Δ and centered in E_i. Fig. 6 illustrates the discontinuity in the behaviour of the vibrational wave-function around the dissociation threshold of the electronic ground state of the molecular ion.

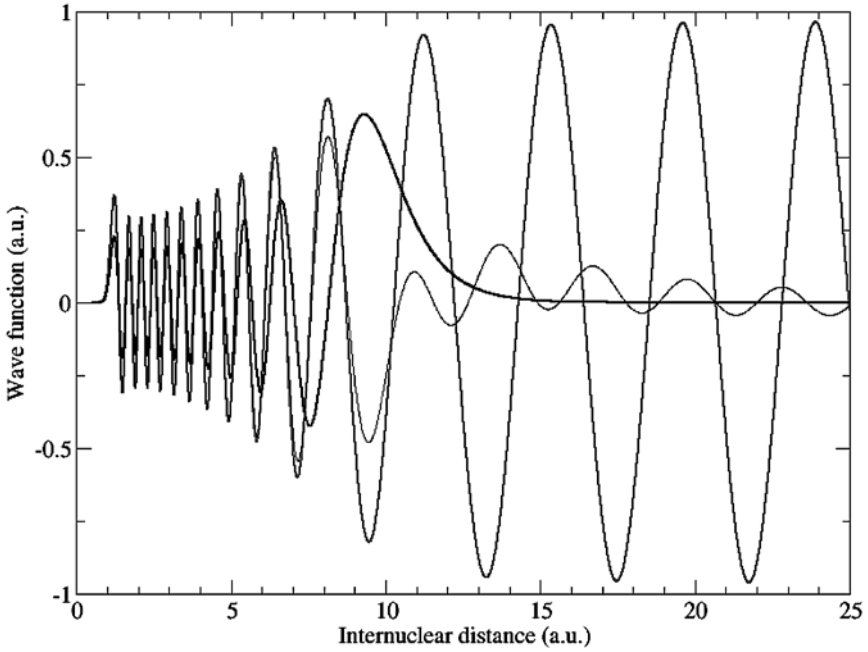

Fig. 6 – Wave functions for the near-threshold vibrational states of HD^+ ($X\ ^1\Sigma_g^+$): black thick line – $v^+ = 21$; grey line – energy-normalized state from the vibrational continuum; thin line – quasi-discretized state from the vibrational continuum (eq. 19).

4. EXAMPLES AND STANDARD RESULTS

Fig. 7 is a sample of the most accurate computation that we are able to perform currently. It concerns the DR of vibrationally relaxed HD^+ ion at very low

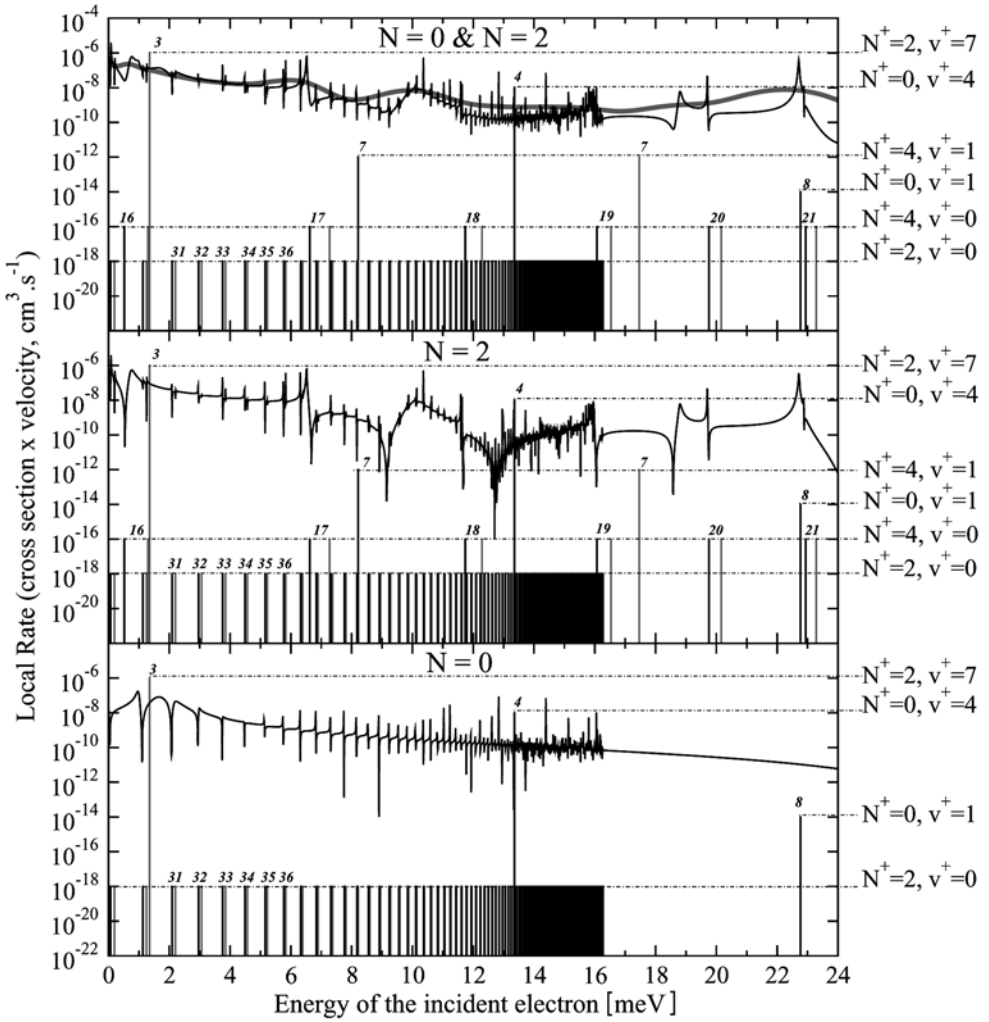

Fig. 7 – Local Rate coefficients (cross section multiplied by relative electron-ion velocity) for DR of ${}^2\Sigma_g^+$ ($N_i^+ = 0$ $v_i^+ = 0$) into the first ${}^1\Sigma_g^+$ dissociative state at low energy. Black curves: MQDT results – for $N = 0$, bottom, $N = 2$, middle and total, top; grey curve: avergage rate, obtained after convolution of the total results with the anisotropic Maxwell distribution in the TSR storage ring [29]. The bars indicate the energies of the predicted resonances for capture of the incident electron into an $l = 2$, "d" (black) or $l = 0$, "s" (grey) Rydberg state. Besides this partial wave index, each expected resonance is labelled by the principal quantum number n and by the rotational and the vibrational quantum numbers, N^+ and v^+ respectively, of the corresponding threshold.

energies of the incident electron. For a given initial rotational level ($N_i^+ = 0$ in Fig. 7), several cases, corresponding to different rotational quantum numbers ($N = 0$ and $N = 2$ in Fig. 7) of the compound neutral system (*HD*), contribute simultaneously. In each of these cases, resonant captures into Rydberg bound states are possible, resulting in resonances in the cross section structure. One can label these resonances, mainly on comparing them to the expected ones according to the Rydberg formula, corresponding to the vertical lines appearing on the graphs. The multichannel aspect appears clearly through the different ro-vibrational (N^+, v^+) thresholds involved in the resonant structure. When a comparison with experimental results is possible, the MQDT result is convoluted with the distribution function of the relative velocity between electrons and ions [29], in order to get the averaged rate-coefficient.

The black curve in the top part of Fig. 7 is just a partial MQDT modelling of a physical situation, like, for example, a collision experiment in a storage ring. Indeed, if one waits some tenth of seconds after the injection of a hetero-nuclear ion beam into the ring, most of the molecular ions will be relaxed vibrationally ($v_i^+ = 0$), but NOT rotationally. It is generally accepted that the rotational levels of such an ion are populated according to the Boltzman law (local thermodynamical equilibrium) corresponding to the rotational temperature of *300 K*. That means that many rotational levels (at least the first 6 or 7 in the case of HD^+) have to be considered as possible initial levels of the target in a reactive collision process. Consequently, for *each* relevant N_i^+ we have to perform *several* (typically 2 or 3) MQDT cross section calculations (each calculation corresponding to a certain total rotational total number *N* accessible via the addition rule of angular momenta, see Table 1 from [33]) and, eventually, perform the Boltzman average of the obtained cross sections. The result of such a calculation is illustrated in Fig. 8 for vibrationally relaxed, but also for weakly vibrationally excited ions. One can notice the very rich resonant structure – coming from super-positions of curves as those appearing in Fig. 7 – due to the indirect process. The importance of this process, as well as of the rotational effects, are clearly demonstrated by the comparison of these results with those obtained after neglecting them (grey curves in Fig. 8).

Rotational calculations are heavy and time consuming. If the experimental resolution is not very high, or if we are interested on the overall behaviour of the rates, or if – as is the case for heavy molecular systems – rotational structure and interactions are not very important, MQDT modelling allowing for vibrational structure and interactions only – *i.e.* neglecting rotation – may be sufficient. But how can we know this in advance? The answer is – at least partially – given in paper [67], although a complete and certain prediction of the importance of the rotational effects is not possible. An example of satisfactory agreement between MQDT modelling and experimental result is given in Fig. 9, where DR rate-coefficient computed for H_2^+ [34] are compared with those measured in the TSR storage

ring [81, 82]. Recent calculations performed in our group, allowing for rotational effects, result in better agreement with the same experiments, but the non-rotational results remain reasonably correct.

Recently, we have performed new calculations on the (still much controversial) HeH^+ DR. As shown in Section 2, we have evaluated the radial coupling responsible for the DR through the C dissociative state using a rigorous extension of the Hellmann-Feynman theorem (Fig. 5). We found no evidence that the non-adiabatic effects could be of comparable magnitude to the electronic ones, as seems to be stated in the study [44]. Therefore, it appears to us that it is possible to overestimate the magnitude of the radial couplings by extrapolating the C-D coupling shown in Fig. 1 of this latter paper, this coupling being the matrix element between states corresponding to the same principal quantum number, $n = 3$. We think that this can not be extrapolated to the continuum. Indeed, the radial coupling elements corresponding to different n values are much smaller (*e.g.* by a factor of 60 in the H_2 case when we compare a 3*s*-3*d* coupling to a 3*s*-4*s* or 3*s*-4*d* one [51]). This explains the difference between the present cross section and the previous one for $^3HeH^+$ [44] plotted in Fig. 10, which was obtained using the C-D coupling extrapolated to the continuum.

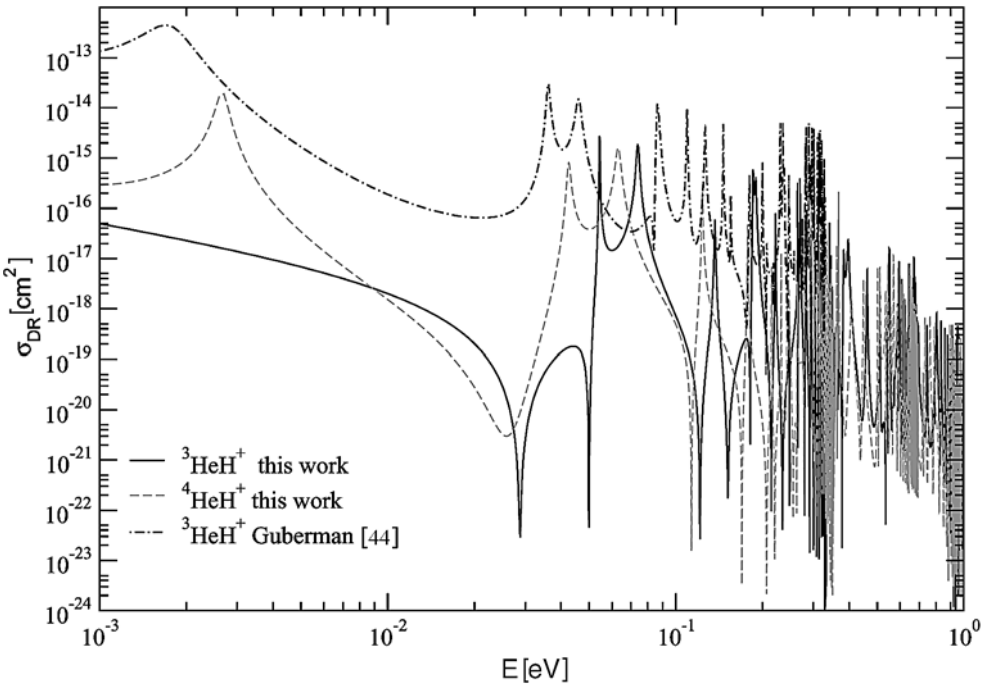

Fig. 10 – Total cross sections for $^3HeH^+$ – full line, this work, dot-dashed line [44] and $^4HeH^+$ – grey dashed line, this work.

Very recently, a complete study of the DR of $^4HeH^+$ was performed by Takagi [47]. His calculation takes into account the rotational motion of the molecule leading to the dynamical mixing of the electronic and nuclear motion. It is the rotation – namely the huge number of ro-vibrational states and the couplings between them – which enhances the DR at low energy – as happens in an another famous "non-crossing" system, H_3^+ / H_3 [64, 85, 86]. As a particular case of his calculation, neglecting the rotation, Takagi obtains DR cross sections of the same magnitude as ours (Fig. 11). The differences between the two results – local shape and resonance positions – are mainly due to the different adiabatic quantum defects used in the two calculations. The overall similar behavior and magnitude of the two "non-rotational" results confirm the validity of the non-adiabatic couplings computed in this work (Fig. 5).

Coming back to systems described appropriately in a quasi-diabatic representation, it is interesting to look to the reactive collisions between electrons and NO^+. In order to contribute to a collisional-radiative model of an air plasma, for hypersonic re-entry and plasma-assisted combustion applications, we performed systematic DR, EC, SEC and IC calculations for the first 15 vibrational levels of the target ion, neglecting rotational effects. Fig. 12 contains a sample of results (a), restricted to low energy (and temperatures) and, most important, a comparison with

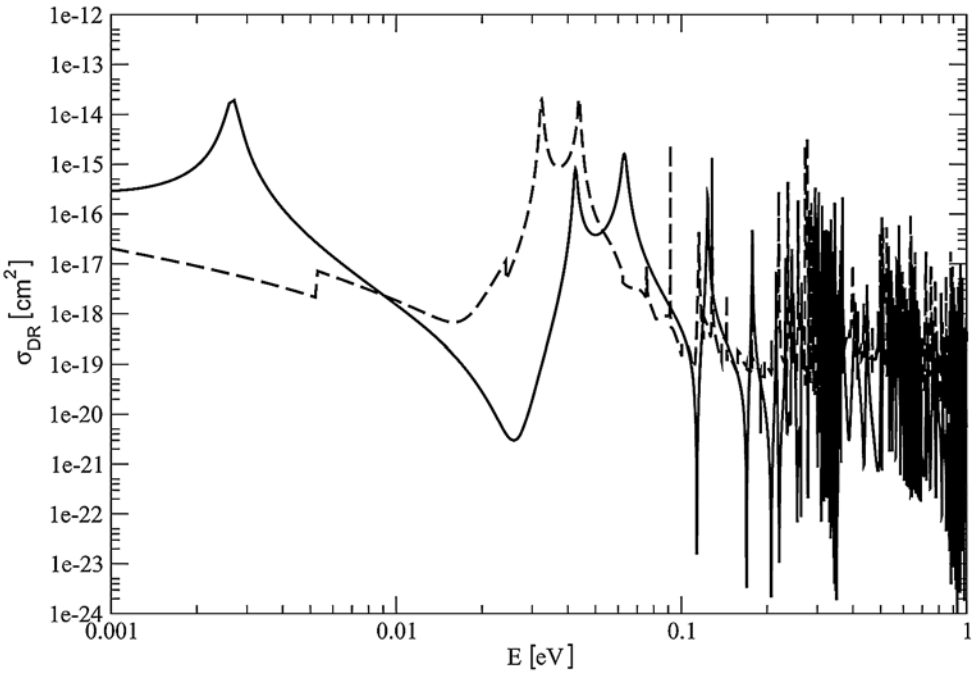

Fig. 11 – Total cross sections for $^4HeH^+$ DR – dashed line [47], full line, present results.

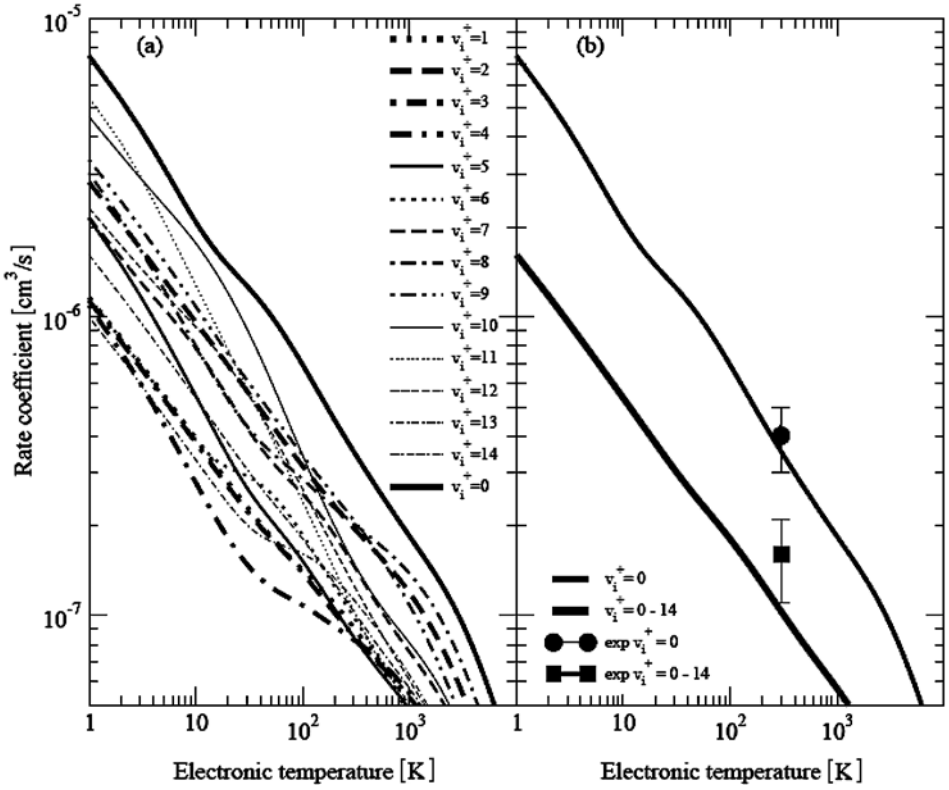

Fig. 12 – NO^+ dissociative recombination. (a) Computed Maxwell isotropic rate coefficient of DR of NO^+ ($X\ ^1\Sigma^+$) initially in its first 15 vibrational levels, as a function of the temperature of the incident electrons. (b) Comparison with the three experimental results: ground state using storage ring [87] and flowing afterglow Langmuir probe [87] techniques in black, and mixture of vibrational states [86] in grey. In the case $v_i^+ = 0$, the two experimental results are very close each to the other: 4×10^{-7} cm^3/s [87] and $(4 \pm 1) \times 10^{-7}$ cm^3/s [87].

three experiments (b), one performed in the ASTRID storage ring [87] and other two using a plasma-type FALP device [87]. The nice agreement shown in this comparison confirms the good quality of the molecular data previously calculated, and shown in Fig. 2.

All the preceding examples deal with the *low energy region*, which can be defined as the energy range of the electron and of the initial ro-vibrational state which correspond to a total energy of the system situated *below* the dissociation limit of the initial electronic state of the molecular ion. Within this region, the "standard" indirect process – temporary captures into bound Rydberg states – is possible, and the cross section displays the typical rich resonant structure appearing in Figs. 6–10.

We shall now illustrate some *high energy* features of the reactive collision processes, restricting ourselves to the case of hydrogen isotopomers. When we

reach the dissociation limit of the molecular ion, its break-up – dissociative excitation (eq. 3) – becomes possible. This process – invoked already at the end of Section 2 and in Fig. 6 – is a generalization of the autoionization (in particular of the vibrational excitation) to the continuum part of the vibrational spectrum of the ion. Consequently, it competes with DR, as shown in Fig. 13, and this competition increases with energy.

Our first DE estimations were in good agreement with previous calculations [84] and measurements [88], as shown in Fig. 14. However, as the energy rises, our approach is no more sufficient, since an other type of dissociative excitation, related to the electronically excited ion core, becomes effective. This process, together with the DR into doubly-excited states having highly-excited cores, are currently under study in our group.

Fig. 15 is a typical output of systematic calculations dedicated mainly to the high-energy electron – HD^+ collisions in the edge plasma of a magnetic fusion device [70]. For each vibrational initial level v_i^+ between 0 and 3, the very low energy (0.01 meV–350 meV) DR calculations have been performed for the first

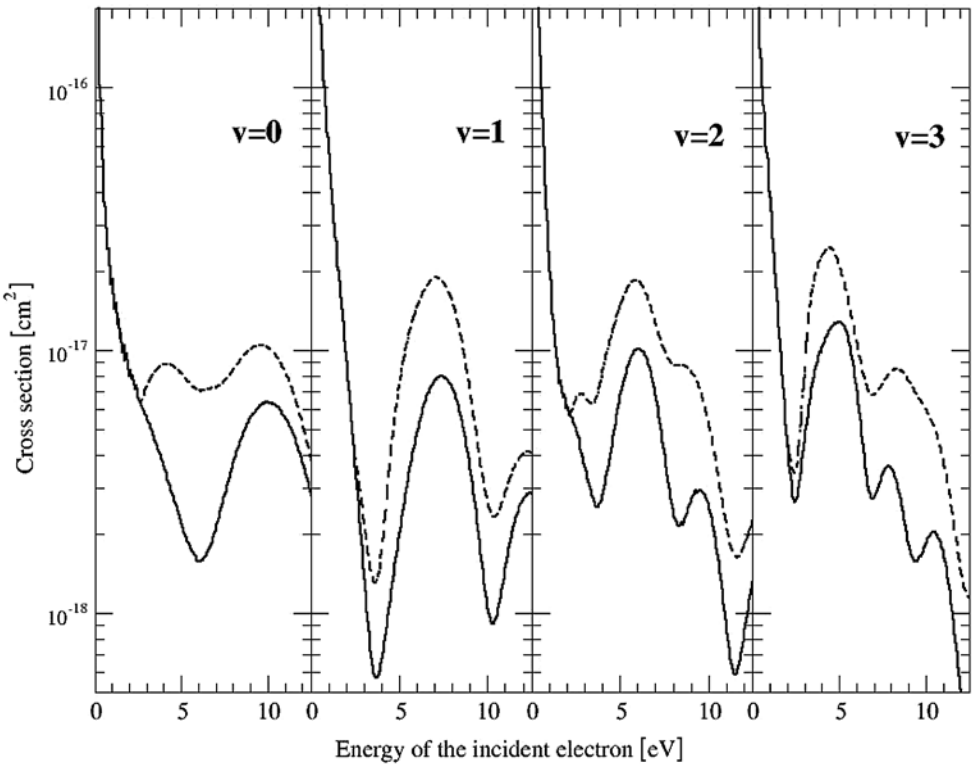

Fig. 13 – Role of the dissociative excitation (DE) on the dissociative recombination (DR) of the HD^+ molecular ion in a given vibrational state v: dashed line – DE neglected, full line – DE included. The contribution of the $^1\Sigma_g^+$ symmetry only was considered in this illustrative case.

13 rotational levels – quite sufficient in the assumption of a 300 K Boltzmann distribution. For a given *initial* rotational level N_i^+ of the ion, all the available total rotational levels N of the neutral (typically 3 values) and all the other rotational levels N^+ of the ion (typically 3 values for every N) accessible via the rules of addition of angular momenta, have been considered in our MQDT calculations [33, 67]. The computations have been performed on an energy grid of 0.01 meV, in order to account for the fine resonances due to the ro-vibrational structure and interactions.

At higher energies, where the direct mechanism was considered for all the five elementary processes, a series of calculations for all the relevant electronic symmetries ($^1\Sigma_g^+$, $^1\Pi_g$, $^3\Pi_g$, $^1\Pi_u$, $^3\Pi_u$, $^1\Sigma_u^+$, $^3\Sigma_u^+$) was performed, for each vibrational quantum number ($v_i^+ = 0, 1, 2, 3$) of the molecular ion target, on an energy grid of 50 meV. The vibrational continuum associated to the ion electronic ground state was discretized using bands of width Δ = 47.1 meV, after preliminary convergence tests.

5. CONCLUSION AND PERSPECTIVES

Almost one hundred years ago, Quantum Mechanics was born from the courageous generalizations of some classical and *macroscopic*-dedicated concepts to the *microscopic* world. One of these concepts was the interference of waves, which, *via* the Schrödinger equation and the subsequent theoretical formalism, is the basis of many physical interpretations and predictions in atomic and molecular physics. In the specific area of the reactive collisions, the quantum interference idea is applied to the multi-channel approach, including the channel mixing phenomenon and, eventually, to the resonant processes. In the present anniversary 2005 WYP context, the rather good agreement between experiment and theory on the electron – cation collisions is one of the numerous arguments in favour of the robust ideas, theories and experiments from the last century, which pushed our knowledge so deeply inside the description of the matter, and allowed many of the current tremendous technological developments.

Our studies aim to a better understanding of the collision processes, including the simplest chemical reactions. Many aspects of these collisions – branching ratios, extension to poly-atomic systems, high energy dissociative excitation, etc. – are still to be addressed. On the other hand, the predictive power of the MQDT method, resulting in cross sections and rate coefficients, contributes to the kinetic modelling of many ionized media, related to challenging projects, as the optimal control of the divertor plasma in the ITER magnetic fusion device, the complete understanding of the particle and energy transfer in the atmospheric re-entry of the spacecrafts, the evolution of various astrophysical and atmospheric environments, and many others.

Acknowledgements. We are grateful to Professor Annick SUZOR-WEINER for introducing us to the MQDT method and its applications, as well as for her constant support and encouragement.

We acknowledge financial support from the IHP programme of the European Union under contract no. HPRN-CT-2000-00141 "Electron Transfer Reactions", from the French CNRS through the "Programme National: Physique et Chimie du Milieu Interstellaire" and from the NATO Orsay-Davis collaboration contract. IFS and MCS are grateful to the French Conseil Régional de la Région Haute Normandie for a postdoctoral grant and for financial support through the project CPER "Combustion dans les moteurs". FOWT acknowledges the financial support of the French Ministère des Affaires Etrangères (SCAC de Yaoundé, Cameroon) for a doctoral grant. IFS is grateful to the French CNRS GdR no. 2495 "Cataplasme". MF, MCS and IFS are grateful to the promoters of the ERASMUS/SOCRATES programme of cooperation between University of Bucharest and Université du Havre. OM is grateful to the "Abdus Salam" International Center for Theoretical Physics, where part of the computations were performed under his Associateship Scheme, and to the Swedish International Development Agency for financial support.

This work has been supported by the International Atomic Energy Agency (IAEA) through the Coordinated Research Project no. F4.30.12 "Data for Molecular Processes in Edge Plasmas".

REFERENCES

1. A. Giusti-Suzor, J. Phys., B **13**, 3687, 1980.
2. M. J. Seaton, Rep. Prog. Phys., **46**, 167, 1983.
3. C. Greene and Ch. Jungen, Adv. At. Mol. Phys., **21,** 51, 1985.
4. Ch. Jungen (editor), *Molecular Applications of Quantum Defect Theory*, IOP, Bristol and Philadelphia, 1996.
5. A. Wolf, L. Lammich and P. Schmelcher (editors), *Sixth International Conference on Dissociative Recombination: Theory, Experiments and Applications*, J. Phys.: Conference. Series, **4**, 2005.
6. A. Bultel and P. Vervisch, J. Phys. B: At. Mol. Opt. Phys., **35**, 111, 2002.
7. A. Bultel, B. van Ootegem, A. Bourdon and P. Vervisch, Phys. Rev., E **65**, 6406, 2002.
8. R. K. Janev, *Atomic and Molecular Processes in Fusion Edge Plasmas*, Plenum, New York, 1995.
9. U. Fantz and P. T. Greenland, Contrib. Plasma Phys., **42**, 694, 2002.
10. R. Schneider, X. Bonnin, N. McTaggart, A. Runov, M. Borchardt, J. Riemann, A. Mutzke, K. Matyash, H. Leyh, M. Warrier, D. Coster, W. Eckstein and R. Dohmen, Comput. Phys. Commun., **164**, 9, 2004.
11. E. Tsitrone, P. Andrew, X. Bonnin, P. Coad, D. Coster, W. Fundamenski, P. Ghendrih, A. Huber, S. Jachmich, A. Kukushkin, A. Loarte, G. Matthews, R. Pitts, J. Rapp, D. Reiter, M. Stamp and M. Ischmeier, Contrib. Plasma Phys., **44**, 241, 2004.
12. M. Wischmeier, R. A. Pitts, A. Alfier, R. Behn, Y. Andrebe, D. Coster, J. Horacek, P. Nielsen, R. Pasqualotto, D. Reiter and A. Zabolotsky, Contrib. Plasma Phys., **44**, 268, 2004.
13. B. Kalache, T. Novikova, I. Fontcuberta, A. Morral, I. Roca, P. Cabarrocas, W. Morscheidt and K. Hassouni, J. Phys., D. Appl. Phys., **37**, 1765, 2004.
14. G. Lombardi, X. Duten, K. Hassouni, M. Capitelli and A. Gicquel, Eur. Phys. J., D At. Mol. Opt. Phys., **30**, 225, 2004.
15. A. Salabas, L. Marques, J. Jolly, G. Gousset and L. L. Alves, J. Appl. Phys., **95**, 4605, 2004.
16. P. Forck, M. Grieser, D. Habs, A. Lampert, R. Repnow, D. Schwalm, A. Wolf and D. Zajfman, Phys. Rev. Lett., **70**, 426, 1993.
17. D. Zajfman, Z. Amitay, C. Broude, P. Forck, B. Seidel, M. Grieser, D. Habs, D. Schwalm and A. Wolf, Phys. Rev. Lett., **75**, 814, 1995.
18. D. Zajfman, Z. Amitay, M. Lange, U. Hechtfischer, L. Knoll, D. Schwalm, R. Wester, A. Wolf and X. Urbain, Phys. Rev. Lett., **79**, 1829, 1997.

19. C. Strömholm, I. F. Schneider, G. Sundström, L. Carata, H. Danared, S. Datz, O. Dulieu, A. Källberg, M. af Uglas, X. Urbain, V. Zengin, A. Suzor-Weiner and M. Larsson, Phys. Rev., A **52**, R4320, 1995.
20. T. Tanabe, I. Katayama, H. Kamegaya, K. Chida, Y. Arakaki, T. Watanabe, M. Yoshizawa, M. Saito, Y. Haruyama, K. Hosono, K. Hatanaka, T. Honma, K. Noda, S. Ohtani and H. Takagi, Phys. Rev. Lett., **75**, 1066, 1995.
21. T. Tanabe, H. Takagi, I. Katayama, K. Chida, T. Watanabe, Y. Arakaki, Y. Haruyama, M. Saito, I. Nomura, T. Honma, K. Noda, and K. Hosono, Phys. Rev. Lett., **83**, 2163–2166, 1999.
22. M. Larsson, L. Bröstrom, M. Carlson, H. Danared, S. Datz, S. Mannervik, and G. Sundstrom, Physica Scripta., **51**, 354, 1995.
23. J. W. Van Der Zande, J. Semaniak, V. Zengin, G. Sundstrom, S. Rosen, C. Stromholm, S. Datz, H. Danared, M. Larsson, Phys. Rev., A **54**, 5010, 1996.
24. H. L. Andersen, J. P. Johnson, D. Kella, B. H. Pedersen and L. Vejby-Christensen, Phys. Rev., A **55**, 2799, 1997.
25. Z. Amitay, A. Baer, M. Dahan, L. Knoll, M. Lange, J. Levin, I. F. Schneider, D. Schwalm, A. Suzor-Weiner, Z. Vager, R. Wester, A. Wolf and D. Zajfman, Science **75**, 5373, 1998.
26. Z. Amitay, A. Baer, M. Dahan, J. Levin, Z. Vager, D. Zajfman, L. Knoll, M. Lange, D. Schwalm, R. Wester, A. Wolf, I. F. Schneider, A. Suzor-Weiner, Phys. Rev., A **60**, 3769, 1999.
27. M. Lange, J. Levin, G. Gwinner, U. Hechttischer, L. Knoll, D. Schwalm, R. Wester, A. Wolf, X. Urbain and D. Zajfman, Phys. Rev. Lett., **83**, 4979, 1999.
28. A. Larson, N. Djuric, W. Zong, H. C. Greene, A. E. Orel, A. Al-Khalili, M. A. Derkatch, A. Le Padellec, A. Neau, S. Rosen, W. Shi, L. Vikor, H. Danared, M. Af Ugglas, M. Larsson and H. G. Dunn, Phys. Rev., A **62**, 042707, 2000.
29. A. Al-Khalili, S. Rosen, H. Danared, M. A. Derkatch, A. Källberg, M. Larsson, A. Le Padellec, A. Neau, J. Semaniak, R. Thomas, M. Af Ugglas, L. Vikor, W. Zong, J. W. Van Der Zande, X. Urbain, J. M. Jensen, R. C. Bilodeau, O. Heber, B. H. Pedersen, C. P. Safvan, L. H. Andersen, M. Lange, J. Levin and G. Gwinner, Phys. Rev., A **68**, 042702, 2003.
30. D. R. Bates, Phys. Rev., A **78**, 492, 1950.
31. J. N. Bardsley, J. Phys. B **1**, 365, 1968.
32. U. Fano, Phys. Rev., **124**, 1866, 1961.
33. I. F. Schneider, C. Strömholm, L. Carata, X. Urbain, M. Larsson and A. Suzor-Weiner, J. Phys. B. At. Mol. Opt. Phys., **30**, 2687, 1997.
34. V. Ngassam, O. Motapon, A. I. Florescu, L. Pichl, I. F. Schneider and A. Suzor-Weiner, Phys. Rev., A **68**, 032704, 2003.
35. V. Sidis and H. Lefebvre-Brion, J. Phys. B At. Mol. Phys., **4**, 1040, 1971.
36. I. Rabadan and J. Tennyson, J. Phys. B: At. Mol. Opt. Phys., **29**, 3747, 1996.
37. I. Rabadan and J. Tennyson, J. Phys. B: At. Mol. Opt. Phys., **30**, 4485, 1997.
38. S. Lepp, P. C. Stancil and A. Dalgarno, J. Phys. B At. Mol. Opt. Phys., **35**, R J57, 2002.
39. W. Roberge and A. Dalgarno, Ap. J., **255**, 489, 1982.
40. M. I. Chibisov and S. I. Yakovlenko, Sov. Phys. JETP, **46**, 21, 1977.
41. A. I. Florescu, V. Ngassam, I. F. Schneider and A. Suzor-Weiner, J. Phys. B At. Mol. Opt. Phys., **36**, 1205, 2003.
42. F. B. Yousif and J. B. A. Mitchell, Phys. Rev., A **40**, 4318, 1989.
43. F. B. Yousif, J. B. A. Mitchell, M. Rogelstad, A. Le Padellec, A. Canosa and V. M. I. Chibisov, Phys. Rev., A **49**, 4610, 1994.
44. S. L. Guberman, Phys. Rev., A **49**, R4277, 1994.
45. S. L. Guberman, in L. Dube, J. B. A. Mitchell, J. W. McConkey and C. E. Brion (editors), *XIXth International Conference on the Physics of Electron and Atomic Collisions*, Whistler, Canada, AIP Conf. Proc., No. **360** , AIP, New York, 307, 1995.
46. S. L. Sarpal, J. Tennyson and L. A. Morgan, J. Phys., B **27**, 5943, 1994.

47. H. Takagih, Phys. Rev., A **70**, 022709, 2004.
48. J. Semaniak, S. Rosen, G. Sundstrom, C. Strömholm, S. Datz, M. Af Ugglas, M. Larsson, W. J. Van der Zande, Z. Amitay, U. Hechtfischer, M. Greiser, R. Repnow, M. Schmidt, D. Schwalm, R. Wester, A. Wolf and D. Zajfman, Phys. Rev., A **54** , R4167, 1996.
49. T. Tanabe, I. Katayama, S. Ono, K. Chida, T. Watanabe, Y. Arakaki, Y. Haruyama, M. Saito, T. Odagiri, K. Hosono, K. Noda, T. Honma and H. Takagi, J. Phys., B **31**, L297-L303, 1998 (corrigendum, J. Phys., B **32**, 5221, 1999).
50. A. I. Florescu, A. Suzor-Weiner, T. Ellinger and F. X. Gadea, Phys. Scripta, **T110**, 172, 2004.
51. A. V. Stolyarov, V. I. Pupyshev and M. S. Child, J. Phys., B. **30**, 3077, 1997.
52. T. Kiyoshima, S. Sato, E. A. Pazyuk, A. V. Stolyarov and M. S. Child, J. Chem. Phys., **118**, 121, 2003.
53. M. C. Van Hemert and S. D. Peyerimhoff, J. Chem. Phys., **94**, 4369, 1991.
54. S. L. Guberman and A. Giusti-Suzor, J. Chem. Phys., **95**, 2602, 1991.
55. R. S. Mulliken, J. Am. Chem. Soc., **86**, 3183, 1964.
56. A. Giusti-Suzor, C. Derkits and J. N. Bardsley, Phys. Rev., A **28**, 682, 1983.
57. M. J. Seaton, Proc. Phys. Soc., **88**, 801, 1966.
58. U. Fano, Phys. Rev., A **2**, 353, 1970.
59. M. Telmini and Ch. Jungen, Phys. Rev., A **68**, 062704, 2003.
60. I. F. Schneider, O. Dulieu, A. Giusti-Suzor, J. Phys. B At. Mol. Opt. Phys., **2**4, L289, 1991.
61. I. F. Schneider, O. Dulieu, A. Giusti-Suzor, Phys. Rev. Lett., **68** (Comment), 2251, 1992.
62. I. F. Schneider, O. Dulieu, A. Giusti-Suzor and E. Roueff, Astrophys. J., **424**, 983, 1994.
63. I. F. Schneider, A. E. Orel, A. Suzor-Weiner, Phys. Rev. Lett., **85**, 3785, 2000.
64. I. F. Schneider, I. Rabadan, L. Carata, L. H. Andersen, A. Suzor-Weiner, J. Tennyson, J. Phys. B At. Mol. Opt. Phys., **33**, 4849, 2000.
65. I. F. Schneider and A. Suzor-Weiner, Contrib. Plasma Phys., **42**, 578, 2002.
66. B. Valcu, I. F. Schneider, M. Raoult, C. Strömholm, M. Larsson, A. Suzor-Weiner, Eur. Phys. J., D **1**, 71, 1998.
67. L. Carata, A. E. Orel, M. Raoult, I. F. Schneider, A. Suzor-Weiner, Phys. Rev., A **62**, 052711, 2000.
68. V. Ngassam, A. I. Florescu, L. Pichl, I. F. Schneider, O. Motapon and A. Suzor-Weiner, Eur. J. Phys., D **26**, 165, 2003.
69. M. C. Stroe, F. O. Waffeu Tamo, M. Fifirig, O. Motapon and I. F. Schneider, submitted to Atomic and Plasma-Material Interaction Data for Fusion, 2005.
70. O. Motapon, M. Fifirig, A. I. Florescu, F. O. Waffeu Tamo, O. Crumeyrolle, G. Varin-Breant, A. Bultel, P. Vervisch, J. Tennyson and I. F. Schneider, submitted to Plasma Sources Science and Technology, 2005.
71. H. Takagi, N. Kosugi, M. Le Dourneuf, J. Phys. B At. Mol. Opt. Phys., **24**, 711, 1991.
72. A. Orel and K. Kulander, Phys. Rev. Lett., **71**, 4315, 1993.
73. I. F. Schneider and A. E. Orel, J. Chem. Phys., **111**, 5873, 1999.
74. A. E. Orel, Phys. Rev., A **62** , 020701, 2000.
75. A. Larson and A. E. Orel, Phys. Rev., A 64, 062701, 2001.
76. A. E. Orel, Journal of Physics: Conference Series, **4**, 142, 2005.
77. J. Tennyson, At. Data Nucl. Data Tables, **64**, 253, 1996.
78. H. J. Takagi, J. Phys. B At. Mol. Opt. Phys., **26**, 4815, 1993.
79. Ch. Jungen and O. Atabek, J. Chem. Phys., **66**, 5584 , 1977.
80. S. Krohn, A. Amitay, A. Baer, D. Zajfman, M. Lange, L. Knoll, J. Levin, D. Schwalm, R. Wester and A. Wolf, Phys. Rev., A **62** , 032713, 2000.
81. S. Krohn, PhD thesis, Max Planck Institut für Kern Physik, Heidelberg, 2001.
82. H. Takagi, in *Dissociative Recombination: Theory, Experiment and Applications III*, editors D. Zajfman, J. B. A. Mitchell and B. Rowe, Word Scientific, Singapore-New Jersey-London-Hong Kong, 174, 1996.

83. H. Takagi, Physica Scripta, **T96**, 52, 2002.
84. I. F. Schneider and A. Suzor-Weiner, Physics Essais, **13**, 280, 2001.
85. V. Kokoouline and C. H. Greene, Phys. Rev., A **68**, 012703, 2003.
86. L. Vejby-Christensen, D. Kella, H. B. Pedersen and L. H. Andersen, Phys. Rev., A **57**, 3627, 1998.
87. T. Mostefaoui, S. Laube, G. Gautier, C. Rebrion-Rowe, B. R. Rowe and J. B. A. Mitchell, J. Phys. B At. Mol. Opt. Phys., **32**, 5247, 1999.
88. D. Zajfman and Z. Amitay, in *Dissociative Recombination: Theory, Experiment and Applications III*, editors D. Zajfman, J. B. A. Mitchell and B. Rowe, Word Scientific, Singapore-New Jersey-London-Hong Kong, 114, 1996.

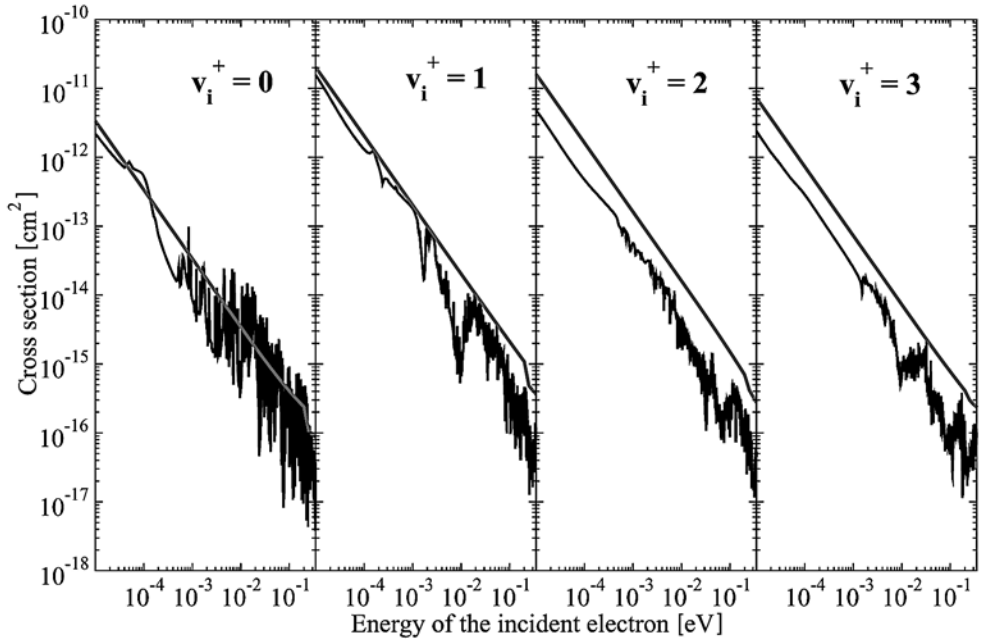

Fig. 8 – Dissociative recombination of HD^+ molecular ion in a given vibrational state v_i^+, at low energy (cross sections). Black line: indirect process and rotational effects included, assuming 300 K rotational thermodynamical equilibrium; grey line: direct process only and rotational effects neglected.

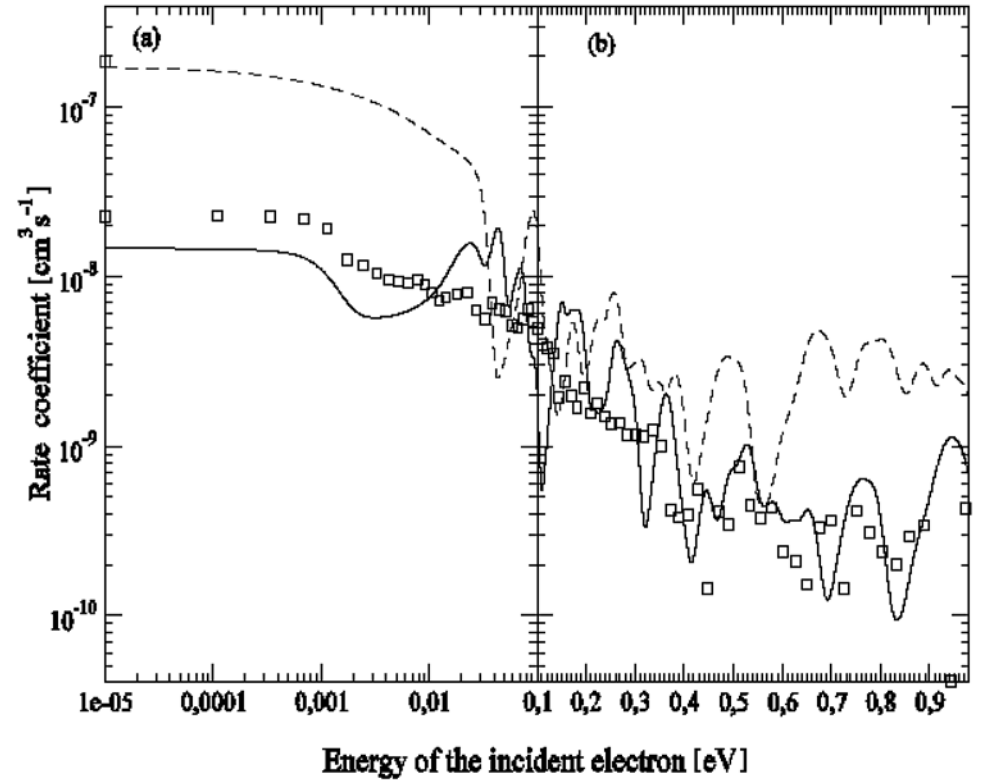

Fig. 9 – Dissociative Recombination of electronically and vibrationally ground state H_2^+. Curves: MQDT calculation for $v_i^+ = 0$ (full) and $v_i^+ = 1$ (grey, dashed). Squares: experiment [81, 82] for $v_i^+ = 0$ (black) and $v_i^+ = 0$ (grey).

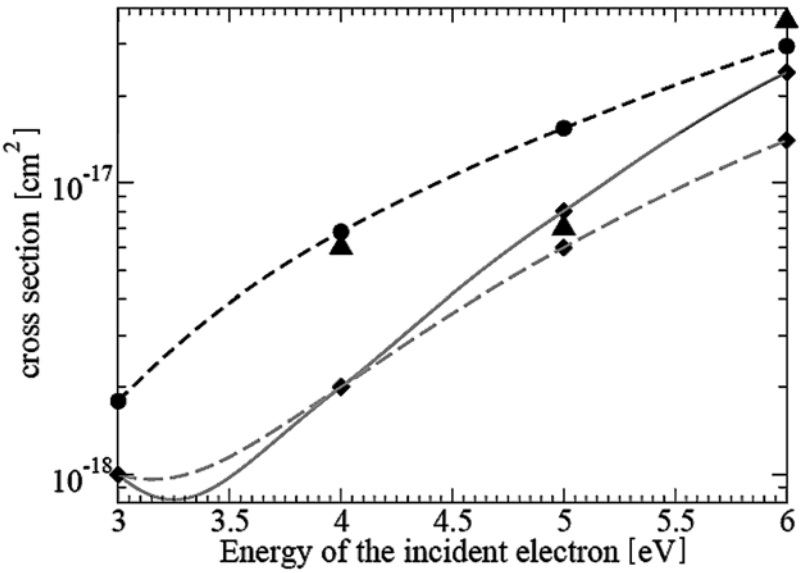

Fig. 14 – Low-energy dissociative excitation of HD^+ ($v_i^+ = 0$). Dashed curves: direct process – black, present work and grey, [84]; solid curve: total process [84]; triangles: TSR storage ring experimental results [88].

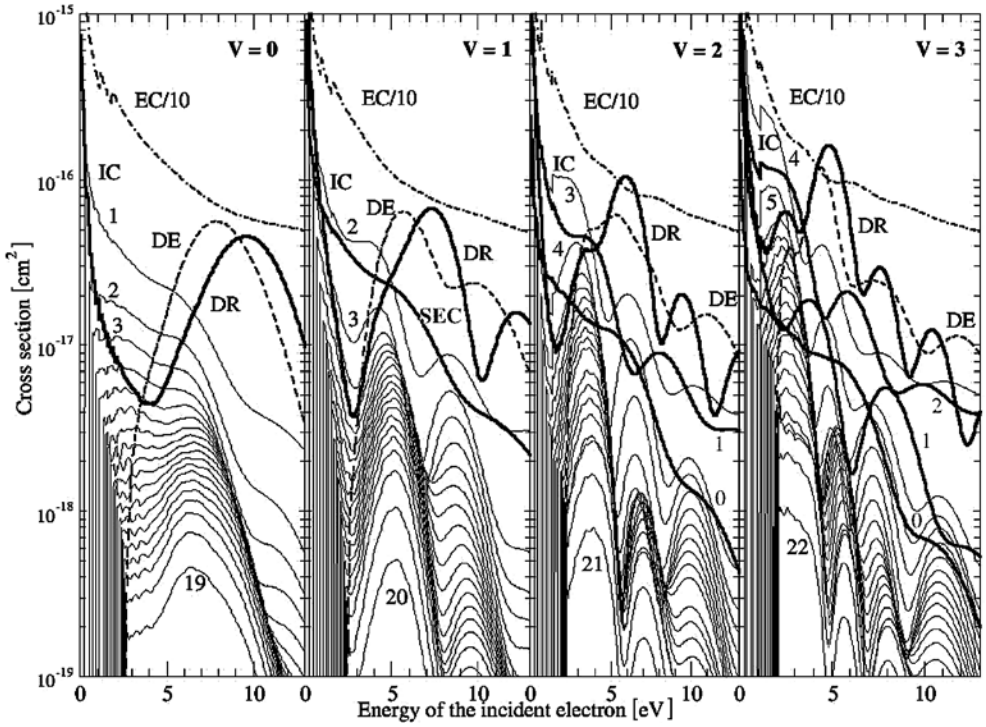

Fig. 15 – Reactive collisions of HD^+ molecular ion in a given vibrational state v with electrons (cross sections): bold line – dissociative recombination (DR), broken line – dissociative excitation (DE), dashed dotted line – elastic collisions (EC), grey line – superelastic collisions (SEC), and thin line – inelastic collisions (IC). The number attached to the IC and SEC curves stand for the final vibrational states.